Article Title:

Study on Shrinkage Deformation of Food in Microwave Vacuum Drying*

Journal name: Drying Technology An International Journal

* This manuscript submission is for **DRT IDS 2014 special issues**.

Corresponding Author: Takaharu TSURUTA, Dr.
Professor of Mechanical Engineering,
Kyushu Institute of Technology,
Sensui 1-1, Tobata-ku, Kitakyushu, Fukuoka 804-8550, JAPAN
E-mail: tsuruta@mech.kyutech.ac.jp
Tel.& Fax: +81 93 884 3140

Co-Author 1: Hirofumi TANIGAWA, Dr.
Assistant Professor of Mechanical Engineering,
Kyushu Institute of Technology
E-mail: tanigawa@mech.kyutech.ac.jp

Co-Author 2: Haruki SASHI, Mr.
Graduate Student of Mechanical Engineering,
Kyushu Institute of Technology
E-mail: o344143t@mail.kyutech.jp

Acknowledgements:

The authors appreciate Mr. A. Kawasaki and K. Ohba for their assistance in this study. This study was partially supported by the Ministry of Education, Science, Sports and Culture, Grant-in-Aid for Scientific Research, Project No. 17360099.

STUDY ON SHRINKAGE DEFORMATION OF FOOD IN MICROWAVE VACUUM DRYING

Abstract

Drying shrinkage is an important problem in the food industry. Focusing on microwave vacuum drying, we study the mechanism of deformation due to shrinkage of the food structure. A relationship between the strain and the water content is introduced for a finite element analysis. The temperature and water distributions are obtained by a finite difference method with the use of a variable permeability and diffusion coefficient depending on the water content. Comparisons with experimental data on radishes, carrots, and tofu indicate that the present model can express the deformation as well as the water content inside the materials.

Keywords: shrinkage deformation, microwave vacuum drying of food, water distribution, MRI imaging, numerical model

INTRODUCTION

The shrinkage of foods during the dehydration processes is an important topic in the food industry and has an impact on the quality of the dried product. The loss of water and heat cause stresses in the cellular structure of food and lead to a change in shape. In general, the drying shrinkage of food materials has a negative effect on the quality of the product. When shrinkage is not uniform during the drying process, there is a possibility of surface cracking of the dried product. Another important consequence of shrinkage is the decrease in the rehydration capability of the product. From these viewpoints, better knowledge of the shrinkage mechanism and the influence of the process variables are needed.

Drying is characterized by the simultaneous transfer of momentum, heat, and moisture and has a significant relationship with modifications in the food structure. There are multiple physics combining the transport and deformation phenomena inside the food being dried. In order to understand the mutual interactions between them, it is effective to create a theoretical model. A comprehensive mathematical model describing the shrinkage phenomenon of materials undergoing drying processes

was first proposed by Kowalski [1]. Several empirical models were also formulated to fit the experimental results and to express the variation in the sample volume with its moisture content. For vegetables, Ratti [2] proposed that the shrinkage characteristics were strictly dependent on the moisture content. Mayor and Sereno [3] summarized the results for convective drying obtained by different authors. Recently, a simultaneous analysis of the transport phenomena and deformation has been carried out with use of numerical simulation for the convective drying [4]. For the case of different drying methods, infrared (IR) drying [5] and combined IR with air drying [6, 7] were also studied.

We have developed a novel microwave vacuum drying system with gas ventilation [8]. Microwave is irradiated so as to keep the temperature of material at room temperatures under the low-pressure conditions. The microwave energy is supplied only for the latent heat to evaporate the water in the material. By introducing a small amount of gas such as air or nitrogen into the drying chamber, water vapor can be removed effectively, and the drying time was shortened successfully. The experimental results with the scallop [8] showed clearly that the gas flow enhanced the evaporation rate in the constant rate period of drying. The surface evaporation rate was 1.6 times as large as the drying without gas supply because the gas flow might reduce the thickness of surface boundary layer and enhance the mass transfer rate. The internal resistance of the water mobility in seafood during microwave vacuum drying was compared with those obtained by warm-air drying, and it was reported that less shrinkage reduces the internal resistance in microwave vacuum drying [9]. Microwave vacuum drying decreased the critical moisture content and increased the period for constant-rate drying. It was clear that controlling the microwave irradiation maintained the material at room temperature and enabled less shrinkage and rapid drying compared to traditional drying methods.

In the present study, we have carried out experimental measurements and numerical simulations focusing on the shrinkage deformation as well as the moisture distribution inside the materials during microwave vacuum drying. A magnetic resonance imaging (MRI) measuring technique is used to observe the distribution of the moisture contents in radishes, carrots, and tofu. To understand the mechanism of deformation due to the shrinkage of the food structure, we have carried out a two-dimensional numerical analysis based on the extended Darcy model for two-phase flow in porous media. The temperature and water distributions are obtained by a finite difference method (FDM) with the use of the relative permeability and diffusion coefficient for the capillary effect depending on

the water content. For the simulation of the drying deformation, we used a finite element analysis by introducing a relationship between the strain and the water content.

EXPERIMENTAL APPARATUS AND PROCEDURES

Microwave vacuum drying system

The experimental apparatus for the microwave-vacuum drying system is shown in Fig.1. The drying principle is the same as microwave vacuum drying, which consists of the vacuum-drying container, vacuum pumping system, and the microwave irradiation equipment. The drying chamber is a cylinder made from stainless steel, which has an inner diameter of 590 mm and a height of 345 mm. The microwave is introduced into the chamber from the side. The microwave generator has a magnetron with a 3-kW irradiation power at 2.45 GHz. We can select intermittent irradiation patterns with a different power as well as continuous irradiation. In order to irradiate the sample uniformly, a turntable is set at the bottom of the chamber. During the experiment, the samples on the table are rotated at a rate of 3 rpm.

We used radishes, carrots, and tofu as the sample materials being dried. Nine pieces of 3 cm cubic samples were used for each material. The drying pressure was set at 5 kPa and the magnetron power was set at 100 W in the present test. Based on the experimental results [8], we introduced nitrogen gas into the drying chamber at a flow rate of 3 L/min in order to enhance the drying rate in the constant rate period of drying. The temperature transients of the samples were measured with fiber-optic thermometers. The moisture content and evaporation rate were obtained from the weight measurement of the sample at several time intervals.

Magnetic resonance imaging of moisture

We observed the moisture distribution inside the sample by using an MRI imaging method. The measurements were performed with a compact MRI system (MR-MIMI-02T, MR Technology, Inc). In the system, a permanent magnet with a field strength of 0.21 T was used to prepolarize protons in water. The sample measurement unit is a cylindrical hole with a diameter of 5 cm or 13 cm. The intensity of the MRI signal was obtained and analyzed using the software Sampler XP-NI with a repetition time of 2000 ms. The 2D-multislice or 3D images were obtained with the imaging software

NMR Imager 3.9. In this paper, we present the 2D distribution of moisture obtained as the average of the 2D-multislice images. Typical images are shown in Fig.2 for a 3-cm cubic radish. The intensity of the signal in various zones of the sample is directly proportional to the water-molecule content [10]. Specifically, darker areas in an image mean that there is less water or a lower number of protons. The relative value of the water content in the sample is obtained from the intensity signal based on the initial water content. The white and black images can monitor the moisture content and its distribution inside the sample.

NUMERICAL METHOD

Heat and moisture transport model for the FDM

In order to obtain the temperature and the water distributions, we have done the two-dimensional numerical analysis by using an FDM. The transport phenomena are analyzed on the basis of the extended Darcy model for two-phase flow inside porous media with use of a simplification of microwave heating.

In microwave vacuum drying, the internal heating by microwaves causes the moisture transport from the inside to the surface, where evaporation takes place [11]. The transport phenomenon inside the porous media is a two-phase flow of liquid water and vapor. Datta [12] presented theoretical approaches for the heat and mass transfer in food processes, and Dincov et al. [13] conducted an electromagnetic analysis of the intensive microwave heating. The penetration depth of a microwave is complicated because the dielectric loss depends on the temperature and moisture content. But it is generally understood that the penetration depth is an order of several centimeters, the electromagnetic analysis is important for larger samples than this size. As the sample size in the present study is a 3-cm cube, we assume uniform microwave power inside the sample (1.5-cm thick) because the half-power penetration depth is about 2cm for pure water at 20^{o}C. It is also assumed that the heat generation by microwaves is proportional to the moisture content because water predominantly absorbs microwave energy [14].

The extended Darcy model expresses the two-phase flow inside a porous material, and the mass-flow rates of each phase are described as follows [15]:

$$\dot{m}_l = -\rho_l \frac{k k_{rl}}{\mu_l} \frac{\partial p_l}{\partial x}, \qquad (1)$$

$$\dot{m}_g = -\rho_g \frac{k k_{rg}}{\mu_g} \frac{\partial p_g}{\partial x}, \qquad (2)$$

where $\dot{m}_l$ and $\dot{m}_g$ are the mean mass-flow rates of the liquid and gas phases, respectively, and *k* is the permeability of the porous structure, and its square value may indicate the characteristic size of the pore. In the extended Darcy model the relative permeability k_{rl} and k_{rg} are introduced to express the flow rate of the liquid and gas phases. It is generally considered that the relative permeability is a function of the moisture saturation *s*, and its value varies between zero and one. Typical formulations of the relative permeability are as follows [16]:

$$k_{rl} = s^m \ , \qquad (3)$$

$$k_{rg} = (1-s)^n \ . \qquad (4)$$

For high-quality drying, moderate heating is preferable. In this case, the gas flow rate can be neglected compared with the liquid, but the capillary effect plays an important role. Therefore, the pressure difference between the gas and the liquid is introduced as the capillary pressure [17]:

$$p_c = p_g - p_l = \frac{\sigma}{\sqrt{k/\varepsilon}} f(s_e) \ . \qquad (5)$$

From Eq. (1) and (5), we obtain the mass-flow rate of moisture as follows:

$$\dot{m}_l = -\rho_l \frac{k k_{rl}}{\mu_l} \frac{\partial p_g}{\partial x} - \rho_l D \frac{\partial s}{\partial x}, \qquad (6)$$

$$D = -\rho_l \frac{k k_{rl}}{\mu_l} \frac{\partial p_c}{\partial s} \ . \qquad (7)$$

That is, the mass flux of the moisture can be expressed separately by the pressure gradient of the gas phase and the diffusion due to the capillary effect.

On the basis of the above consideration, we have carried out a two-dimensional numerical analysis of the heat and moisture transfer. The fundamental equations are as follows:

$$\rho_l \varepsilon \frac{\partial s}{\partial t} = -\frac{\partial \dot{m}_{lx}}{\partial x} - \frac{\partial \dot{m}_{ly}}{\partial y}, \qquad (8)$$

$$\dot{m}_{lx} = -\rho_l \frac{k k_{rl}}{\mu_l} \frac{\partial p_g}{\partial x} - \rho_l D \frac{\partial s}{\partial x}, \qquad (9)$$

$$\dot{m}_{ly} = -\rho_l \frac{k k_{rl}}{\mu_l} \frac{\partial p_g}{\partial y} - \rho_l D \frac{\partial s}{\partial y}, \qquad (10)$$

$$\frac{\partial}{\partial t}\left\{(\rho c_p)_T T\right\} = \frac{\partial}{\partial x}\left(\lambda \frac{\partial T}{\partial x}\right) + \frac{\partial}{\partial y}\left(\lambda \frac{\partial T}{\partial y}\right) - \frac{\partial}{\partial x}\left(\dot{m}_{lx} c_{pl} T\right) - \frac{\partial}{\partial y}\left(\dot{m}_{ly} c_{pl} T\right) + \dot{q}_g \cdot s, \quad (11)$$

where $\dot{q}_g$ is the rate of water heating by the microwave per unit volume. In the case of no water content ($s = 0$), there is no heat generation. As noted before, we assume a linear relationship between the volumetric heating rate and the water content in Eq. (11). Because the thermal conductivity and the heat capacity depend on the water content, we used the weighted averaging with the ratio of solid matrix and liquid phase. For the relative permeability k_{rl} and moisture diffusion coefficient D, cubic functions of the moisture saturation s were utilized

$$k_{rl} = s^3, \quad (12)$$

$$D = D_{eff} \cdot s^3, \quad (13)$$

where D_{eff} is the effective diffusion coefficient that expresses the capillary effect, and we assume $D_{eff} = 10^{-7}\ m^2/s$ in this study.

For the surface boundary conditions, the evaporation rate per unit area $\dot{m}_e$ was approximated by the following equation with use of the mass transfer coefficient h_D and the ideal gas assumption:

$$\dot{m}_e = \rho_g h_D (\omega - \omega_\infty) \approx \frac{\rho_g h_D}{P}\left(p_w - \varphi \cdot p_{s\infty}\right). \quad (14)$$

The value of the mass transfer coefficient was set as $h_D = 0.02\ m/s$, which is actually estimated by the measurement of the evaporation rate of pure water in the container under the same conditions as the microwave vacuum drying of food. Considering the transport of latent heat L due to the evaporation, the following equation is used as the boundary condition for the energy:

$$-\lambda \left.\frac{\partial T}{\partial x}\right|_{surface} = -\varepsilon \dot{m}_e L. \quad (15)$$

An FDM was used for a square 2D sample with a side length of 30 mm. The initial temperature was set at 20 °C, and the initial moisture content was unity. The ambient temperature and pressure were fixed at 20 °C and 5 kPa, respectively. The heating rate $\dot{q}_g$ by microwave irradiation was set at 300 kW/m^3. Other parameters such as the thermal properties of the materials are listed in Table 1.

Shrinkage deformation model for the FEM

For the estimation of the shape variations of the food being dried, the heat and moisture transport equations should be coupled to the structural mechanics. Yang et al. [18] proposed a model describing the deformations due to moisture removal. They assumed that the deformation behavior was elastoplastic within a small strain region and considered that the strain displacement was proportional to the moisture removal. In this study, the model of Yang et al. is utilized for the numerical simulation using a finite element method (FEM) for the shrinkage deformation during drying.

According to Yang et al, the local total strains $\{d\varepsilon\}$ are related to the changes in both the mechanical strains $\{d\varepsilon_m\}$ and shrinkage strains $\{d\varepsilon_s\}$ due to the moisture loss ds:

$$\{d\varepsilon\} = \{d\varepsilon_m\} + \{d\varepsilon_s\} = \{d\varepsilon_m\} + \alpha \cdot ds, \qquad (16)$$

where α is the shrinkage coefficient. The stress–strain relationship is expressed through the elastic stress–strain matrix, which accounted for the Young modulus E and the Poisson ratio υ. In addition, the strain–displacement relationship is formulated in the triangular element system in the FEM:

$$\{\sigma\} = [D]\{\varepsilon\}, \qquad (17)$$

$$\{\varepsilon\} = [B]\{u\}, \qquad (18)$$

where $[D]$ and $[B]$ are the elastic and displacement matrices, respectively. The displacement vector $\{u\}$ is obtained from the stiffness equation:

$$[K]\{u\} = \{F\}, \qquad (19)$$

where $[K]$ is the stiffness matrix, and $\{F\}$ is the force vector. The stiffness matrix is obtained by the summation of the elemental stiffness matrix:

$$[K] = \sum\{k\} = \sum[B^t][D][B]\Delta, \qquad (20)$$

where Δ is the area of the triangular element in the FEM. This analytical method for the FEM is similar to the thermo-elastoplastic analysis, and the details can be found in [19].

RESULTS AND DISCUSSION

Experimental results for the drying characteristics and shrinkage coefficient

The shrinkage coefficient α in Eq. (16) was measured during the microwave vacuum drying. Figure 3 shows the drying characteristic and shrinkage behavior of a radish. In Fig.3 (a), the drying

rate is expressed as a function of the relative moisture content, where the measured data for nine pieces were plotted within a repetition of ±20% from the average. We can clearly observe two types of drying periods: the constant-rate period (CRP) and the falling-rate period (FRP). It is found that the critical moisture content is approximately 0.25 as a dimensionless value. In the present study, the moisture content is expressed in a dimensionless form on the basis of the initial moisture content. The critical water contents with dimensions (g/g-dry base) are summarized with the initial moisture contents of samples in Table 2.

Most previous studies have discussed the relationship between the ratio of the volume to the initial volume and the moisture content [3]. Following this viewpoint, Fig.3 (b) shows the volume shrinkage as a function of the moisture content. A linear relationship is observed over the entire range of water content within ±10%, and a marked change is not observed before and after the critical moisture content. However, it was reported that the linearity is lost if development of the porosity changes sharply during the final stage of drying after the critical moisture content. Further, considering that the tensor matrix formulates the stress–strain relationship, we have plotted the cubic root of the volume ratio instead of the volume change in Fig.3 (c). A different dependency on the moisture content is clearly observed between the constant rate period and the falling rate period. Therefore, we propose a shrinkage coefficient as the gradient of a fitting line expressing the relationship between the cubic root of the volume ratio and the moisture content with ±5% uncertainties as shown in Fig.3 (c). That is, we define the shrinkage coefficient α by the following equation:

$$\sqrt[3]{\frac{V}{V_0}} = \alpha \frac{\Delta S}{S_0} \approx \frac{L}{L_0}. \qquad (21)$$

Table 2 summarizes the shrinkage coefficients during each drying period for the radish, carrot, and tofu together with the initial and critical moisture contents. For the carrot, two types of shrinkage coefficients are obtained because of the structural differences between the center and outer regions. The center area exhibits a larger shrinkage coefficient during the falling-rate drying period.

Shape deformation and moisture content distribution

First, the drying deformation of the carrot and tofu is examined experimentally and numerically. Figure 4 shows the experimental and numerical results for comparisons of the shape, moisture, and

temperature distributions around the critical moisture content of 0.31. The initial shape is a cube with a side length of 30 mm. In the figures, (a) the external appearance and (b) the MRI of the water distribution are compared with (c) and (d) from the numerical results.

For the carrot, the cubic shape shrinks to the corner-shaped form, as seen in Fig.4 (a). The MRI clearly points out less moisture content at the central region. In addition, there is smaller water content at just the surface, yet a large amount of water is kept near the surface. It is considered that the corner area enhances the surface evaporation because of the large evaporation area and the considerable energy absorption due to the microwave heating of water. This indicates moisture perfusion from the center to the corner surface. The numerical shape and moisture distribution agree with the experimental results.

Contrary to the carrot, the tofu exhibits an entirely different shape and moisture distribution. The appearance of tofu looks like a round shape, and the central region has a larger moisture content. The numerical simulation also shows similar results.

For a detailed comparison of the moisture distributions between the experimental and numerical results, Fig.5 shows the moisture profiles at the central cross section of the carrot and tofu. The abscissa corresponds to the vertical position from the bottom of the sample shown in Fig.4. The experimental moisture distributions were obtained by the MRI measurements that include an uncertainty of ±15% in the calibrations. As noted before, the moisture content at the center region of the carrot is lower than the near-surface portion. It is also found that the moisture content decreases sharply at the surface. This indicates rapid evaporation at the surface, resulting in surface shrinkage, similar to a skin effect. In the inner portion, moisture transport occurs in a negative direction to the gradient of the moisture content, which indicates that the pressure difference plays an important role in moisture transport during microwave vacuum drying. The sharp decrease in the moisture content at the surface is also observed in the tofu, but the moisture distribution at the inner portion is almost uniform, as seen in Fig.5 (b). This is because tofu has a much smaller permeability than the carrot. The comparisons in Fig.5 show relatively good agreement between the numerical results and the MRI measurements, whereas the simulations cannot express the asymmetric behaviors observed in the experiments.

Finally, the shrinkage behavior of the radish is shown in Fig.6. As seen in the appearances in

Fig.6 (a), the radish changes its form to a flattened shape at the final stage of drying. The longer side direction coincides with the fiber direction of the radish. This reminds us of an inhomogeneous shrinkage coefficient due to the fibrous structure of the radish. In Fig.3, we measured the volume change and estimated the shrinkage coefficient $\alpha = 1.21$ for the stage of falling-rate drying. However, it is necessary to consider the anisotropic inhomogeneity caused by the fibrous structure in order to express the experimental results of the flattened shape. Therefore, we have measured the shrinkage coefficients for different directions, i.e., the fibrous and orthogonal directions: $\alpha_{//} = 1.0$ and $\alpha_{\perp} = 1.4$, respectively. With use of these different shrinkage coefficients, numerical simulations have been carried out, and the results are shown in Fig.6 (b). The simulation results agree with the experimental shapes well, even for the final stage of drying. Therefore, it is concluded that a directional shrinkage coefficient is necessary to express the shrinkage phenomena precisely. From this viewpoint, the definition of the shrinkage coefficient in Eq. (21) is important.

CONCLUSIONS

Focusing on the relationship between the shrinkage deformation and the moisture distribution of food, MRI measurements and numerical simulations have been carried out for the process of microwave vacuum drying of radishes, carrots, and tofu. The MRI images of the moisture distribution clearly indicated that the central part of the samples dehydrated faster than the outer region, except for the surface layer. The surface formed a skin layer with less moisture content and more shrinkage, even in microwave vacuum drying. By introducing a shrinkage coefficient defined with an experimental relationship between the cubic root of the volume ratio and the moisture content, FEM analyses were then carried out in this study. Coupled with the FDM analyses of the heat and moisture transport phenomena based on the extended Darcy model, the shrinkage deformation and moisture distribution have been studied numerically. The simulation results show good agreement qualitatively with the experimental measurements. It is found that the vapor pressure drives the moisture from the inner to the surface because of the internal heating by microwave irradiation. Concerning drying deformation, the present model can express the experimental results if we use the shrinkage coefficient defined by the cubic root of the volume ratio. This is because the shrinkage behavior changes before and after the critical moisture content. It is also recommended to consider the directional shrinkage coefficient for

food with a fibrous structure.

ACKNOWLEDGEMENTS

The authors appreciate Mr. A. Kawasaki and K. Ohba for their assistance in this study. This study was partially supported by the Ministry of Education, Science, Sports and Culture, Grant-in-Aid for Scientific Research, Project No. 17360099.

REFERENCES

1. Kowalski, S.J. Mathematical modeling of shrinkage during drying. Drying Technology 1996, 14 (2), 307-331.

2. Ratti, C. Shrinkage during of foodstuffs. Journal of food engineering 1994, 23 (1), 91-105.

3. Mayor, L.: Sereno, A.M. Modelling shrinkage during convective drying of food materials: a review. Journal of food engineering 2004, 61 (3), 373-386.

4. Curcio, S.; Aversa, M. Influence of shrinkage on convective drying of fresh vegetables: a theoretical model. Journal of food engineering 2014, 123 (2), 36-49.

5. Timoumi, S.; Mihoubi, D.; Zagrouba, F. Shrinkage, vitamin C degradation and aroma losses during infra-red drying of apple slices. LWT 2007, 40 (9), 1648-1654.

6. Mihoubi, D.; Timoumi, S.; Zagrouba, Modelling of convective drying of carrot slices with IR heat source. Chemical Engineering and Processing 2009, 48 (3), 808-815.

7. Ponkham K.; Meeso, N.; Soponronnarit, S.; Siriamornpun, S. Modeling of combined far-infrared radiation and air drying of a ring shaped-pineapple with/without shrinkage. Food and Bioproducts Processing 2012, 90 (2), 155-164.

8. Tsuruta, T.; Hayashi, T. Enhancement of microwave drying under reduced pressure condition by irradiation control and external air supply. In Proceedings of the Third Nordic Drying Conference NDC2005, Karlstad, Sweden, June 15-17, 2005; CD-Rom 8 pages.

9. Tsuruta, T.; Hayashi, T; Internal resistance to water mobility in seafood during warm air-drying and microwave-vacuum drying. Drying Technology 2007, 25 (7-8), 1393-1399.

10. Marcone, MF; Wang, S.; Albabish, W.; Nie, Shaoping; Somnarain, D; Hill, A. Diverse Food-Based Applications of Nuclear Magnetic Resonance (NMR) Technology, Food Research International 2013, 51 (2), 729–747.

11. Turner, I.W; Jolly, P. Combined Microwave and Convective Drying of a Porous Material. Drying Technology 1991, 9 (5), 1209–1270.

12. Datta, AK. Porous media approaches to studying simultaneous heat and mass transfer in food processes. I: problem formulations. Journal of Food Engineering 2007, 80 (1), 80–95.

13. Dincov, DD; Parrott, KA; Pericleous, KA. Heat and mass transfer in two-phase porous materials under Intensive microwave heating. Journal of Food Engineering 2004, 65 (3), 403–412.

14. Ni, H.; Datta, A. K.; Torrance, K. E. Moisture transport in intensive microwave heating of biomaterials: A multiphase porous media model. International Journal of Heat and Mass Transfer 1999, 42 (8), 1501–1512.

15. Scheidegger, A. E. The Physics of Flow Through Porous Media, 3rd ed.; University of Toronto Press, 1974; 245–269.

16. Kawamura, H.; Hijikata, K. Simulation of Heat and Flow (in Japanese); Maruzen, 1995; 165–185.

17. Wan, C. Y.; Cheng, P.; Multiphase Flow and Heat Transfer in Porous Media, Advances in Heat Transfer, Academic Press, 1997, 30, 93–196.

18. Yang, H.; Sakai, N.; Watanabe, M. Drying model with non-isotropic shrinkage deformation undergoing simultaneous heat and mass transfer. Drying Technology 2001, 19 (7), 1441-1460.

19. Tanaka, K.; Nagaki, S.; Inoue, T. Theory of Elasticity and Finite Element Method; Taiga Press, Tokyo, 2006.

20. Souma, S.; Tagawa, A.; Iimoto, M.; Effects of Structural Properties Change During Drying on Thermal Conductivity of Fruits and Vegetables. Nippon Shokuhin Kagaku Kougaku Kaishi, 2004, Vol.51, No.8, 428-434.

21. Japan Society of Thermophysical Properties, Thermophysical Properties Handbook, YOKENDO, 2008.

22. Nuri N. Mohsenin , Thermal Properties of Food and Agricultural Materials, KOURIN, 1985

23. Murata, S; Koide, S; Temperature Dependency of Young’s Modulus and Poisson’s Ratio of Agricultural and Food Materials – Measuring Under Both Ends Fixed Boundary Condition – , Journal of the Japanese Society of Agricultural Machinery, 1994, 56(6), 41-49.

List of figures and tables

Figure captions

Figure 1 Microwave vacuum drying system.

Figure 2 MRI images of the moisture distribution inside a radish.

Figure 3 Drying characteristic curve and shrinkage behavior of the radish.

Figure 4 Comparison between experiments and numerical simulations for the shape, moisture, and temperature distributions for a moisture content of 0.31.

Figure 5 Comparison of moisture distribution at the center plane.

Figure 6 Shrinkage behaviors of a radish.

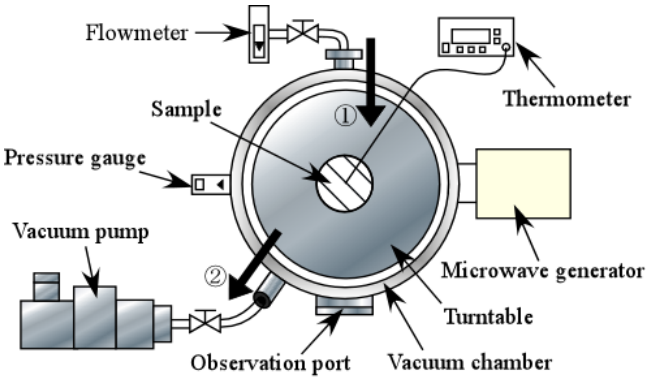

Figure 1 Microwave vacuum drying system.

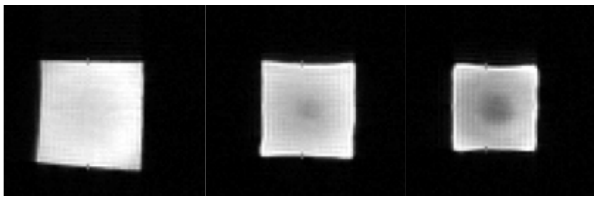

(a) 17.5 g/g-dry (100%)　(b) 12.0 g/g-dry (68.8%)　(c) 8.65 g/g-dry (49.4%)

Figure 2　MRI images of moisture distribution inside a radish.

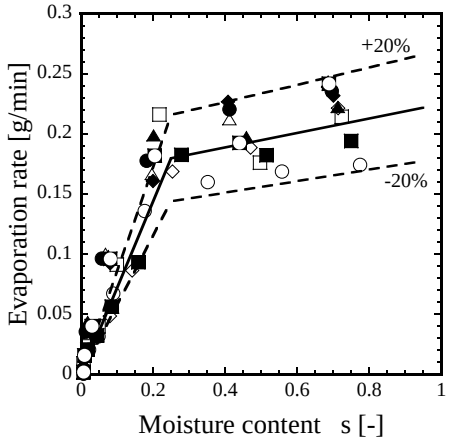

(a) Drying characteristics

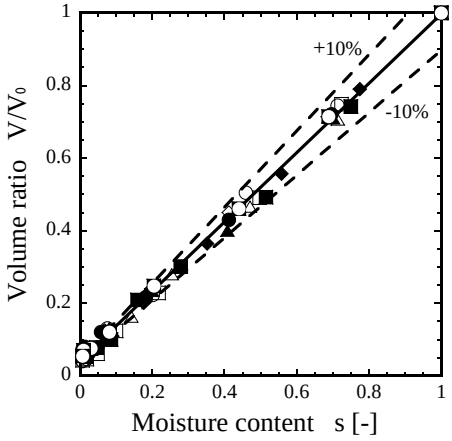

(b) Volumetric change

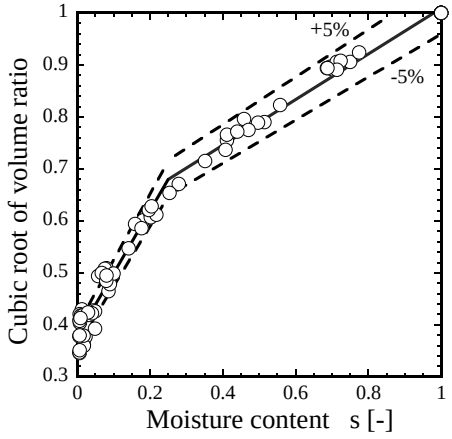

(c) Cubic root of volumetric change

Figure 3 Drying characteristic curve and shrinkage behavior of the radish.

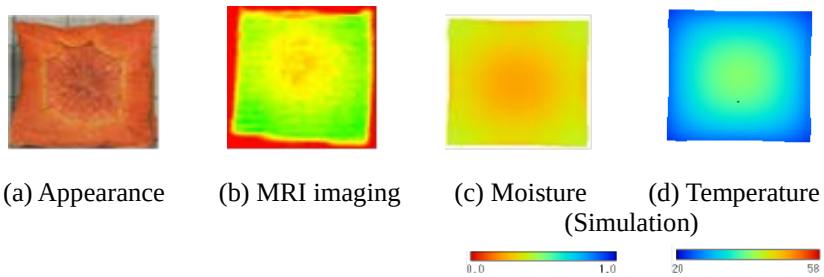

(a) Appearance (b) MRI imaging (c) Moisture (d) Temperature (Simulation)

(a) Carrot

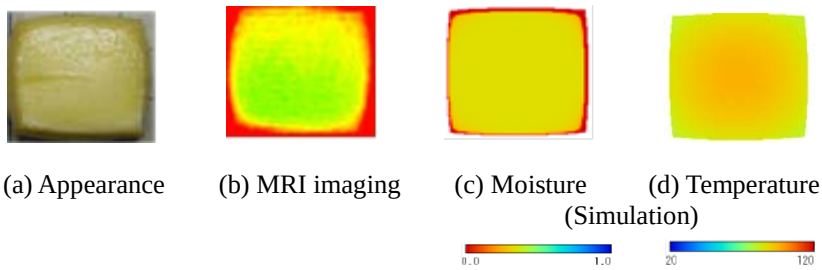

(a) Appearance (b) MRI imaging (c) Moisture (d) Temperature (Simulation)

(b) Tofu

Figure 4 Comparison between experiments and numerical simulations for the shape, moisture, and temperature distributions for a moisture content of 0.31.

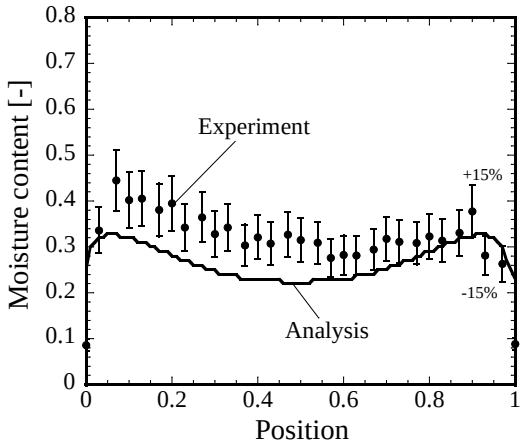

(a) Carrot

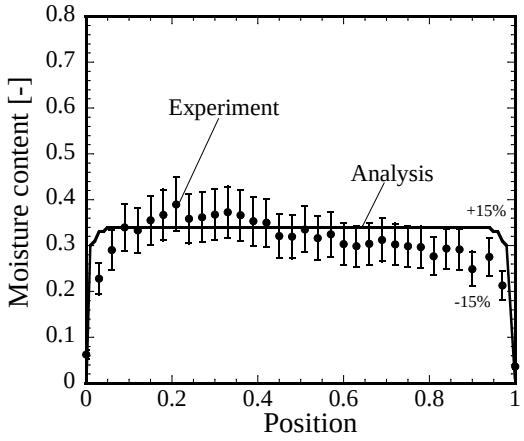

(b) Tofu

Figure 5 Comparison of the moisture distribution at the center plane.

s = 1.00 s = 0.46 s = 0.17 s = 0.07

(a) Experiment

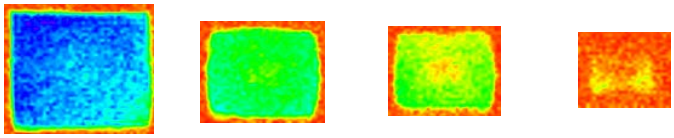

s = 1.00 s = 0.46 s = 0.17 s = 0.07

(b) MRI imaging

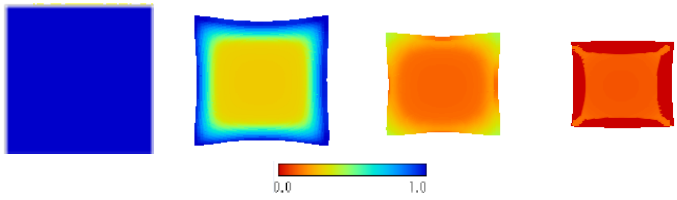

s = 1.00 s = 0.46 s = 0.17 s = 0.07

(c) Moisture distribution (simulation)

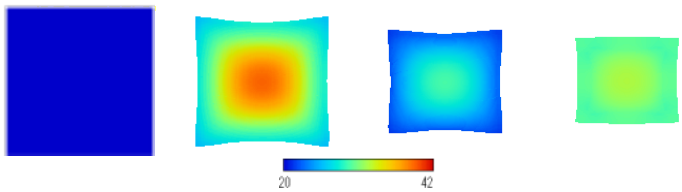

s = 1.00 s = 0.46 s = 0.17 s = 0.07

(d) Temperature distribution (simulation)

Figure 6 Shrinkage behaviors of a radish.

Table captions

Table 1 Numerical conditions for the FDM and FEM.

Table 2 Drying and shrinkage characteristics.

Table 1 Numerical conditions for the FDM and FEM.

Material	Radish	Carrot	Tofu
Density, ρ (kg/m^3)	1460.9	1481.9	2083.3
Specific heat, c_p (J/(kgK))	1008[(b)]	1730[(b)]	1577[(c)]
Porosity, ε	0.95	0.90	0.90
Thermal conductivity, λ (W/(mK))	0.00492[(a)]	0.0361[(a)]	0.0900
Young's modulus, E (N/mm^2)	2.0	5.08/4.50	0.01
Poisson's ratio, ν (-)	0.394[(d)]	0.300[(d)]	0.300
Permeability, k (μm^2)	0.05	0.01	0.001

(a) ref.[20], (b) ref.[21], (c) ref.[22], (d) ref.[23]

Table 2 Drying and shrinkage characteristics.

Material	Radish	Carrot	Tofu
Initial moisture content, g/g-dry	23.27	10.39	7.29
Critical moisture content, g/g-dry	5.82	3.12	2.55
in dimensionless form	0.25	0.30	0.35
Shrinkage coefficient in CRP	0.44	0.49/0.50	0.43
in FRP	1.21	1.02/0.89 (center/outer)	0.79